

Variational quantum computation with discrete variable representation for ro-vibrational calculations

K. Asnaashari,^{a)} D. Bondarenko, and R. V. Krems

*Department of Chemistry, University of British Columbia,
Vancouver, B.C. V6T 1Z1, Canada
Stewart Blusson Quantum Matter Institute,
Vancouver, B.C. V6T 1Z4, Canada*

(Dated: 15 October 2024)

We demonstrate an approach to computing the vibrational energy levels of molecules that combines the discrete variable representation (DVR) of molecular Hamiltonians with variational quantum eigensolvers (VQE) and a greedy search of optimal quantum gate sequences. We show that the structure of the DVR Hamiltonians reduces the quantum measurement complexity scaling from exponential to polynomial, allowing for efficient VQE without second quantization. We then demonstrate that DVR Hamiltonians also lead to very efficient quantum ansatze for representing ro-vibrational states of molecules by states of a quantum computer. To obtain these compact representations, we demonstrate the quantum ansatz search by computing the vibrational energy levels of Cr_2 in seven electronic states as well as of van der Waals complexes $\text{Ar}-\text{HCl}$ and $\text{Mg}-\text{NH}$. Our numerical results show that accuracy of 1 cm^{-1} can be achieved by very shallow circuits with 2 to 9 entangling gates.

I. INTRODUCTION

Accurate calculation of molecular properties is considered a promising application of quantum computing. The eigenstates of molecular Hamiltonians can be obtained on quantum computers by variational quantum eigensolvers (VQEs)^{1,2} that employ sequences of gates operating on qubits (quantum circuits) to prepare quantum states tailored for specific problems. VQEs have been applied for solving the electronic structure problem for molecules^{3–11} and lattice models^{1,7,12}. However, applications of VQE to computations of ro-vibrational energies and states have been limited^{13–20}. Refs.^{16,17} demonstrated a general approach for computing ro-vibrational energy levels of polyatomic molecules inspired by previous work on electronic structure. However, the methods of Refs.^{16,17} require extended quantum circuits including > 200 ¹⁷ or between 44 and 140 292¹⁶ entangling gates. A key challenge for quantum computing of molecular dynamics is to develop a general approach that can (i) be applied to a wide variety of ro-vibrational states, from deeply bound to van der Waals states; (ii) yield high accuracy with shallow quantum circuits; (iii) exhibit at most a polynomial scaling with the dimensionality of the molecular configuration space. Within VQE, (i) requires an ansatz for quantum circuits that can represent molecular states in widely varying landscapes of potential energy; (ii) is necessary due to noise and hardware limitations of current quantum computers; and (iii) is required for the quantum advantage.

Here, we formulate a general approach to computing the ro-vibrational energy levels of molecules with VQE based on discrete variable representations (DVR) of molecular Hamiltonians^{21,22}. We first derive the theoretical bounds on the quantum measurement complexity with VQE based on general DVR. Our analysis shows that the structure of the DVR Hamiltonians reduces the quantum measurement complexity scaling from exponential to polynomial.

In the second part of this work, we demonstrate that DVR Hamiltonians also lead to very efficient quantum ansatze for representing ro-vibrational states of molecules by states of a quantum computer. To do this, we develop a compositional search algorithm that explores the space of gate permutations to yield quantum circuits suitable for ro-vibrational VQE computations. To illustrate the generality of this approach and the efficiency of the resulting quantum circuit representations of ro-vibrational states, we consider Cr_2 in seven different electronic states²³ and van der Waals complexes $\text{Ar}-\text{HCl}(^1\Sigma)$ and $\text{Mg}-\text{NH}(^3\Sigma)$. These molecular systems exhibit ro-vibrational states with widely different energies (from -55 to $-15,000 \text{ cm}^{-1}$ from the dissociation threshold) and spatial variations of wave functions and energy level patterns. Our greedy compositional search yields quantum circuits that produce VQE results with accuracy $< 1 \text{ cm}^{-1}$ for ground and excited ro-vibrational energy levels, illustrating the ability of VQE to compute the rotational constants and vibrational anharmonicity, with between 2 and 9 entangling gates.

The remainder of this article is organized as follows. After a brief introduction of VQE, Section II A

^{a)}Electronic mail: kasra.asnaashari@phys.chem.ethz.ch

presents an algorithm to evaluate the DVR Hamiltonians with a polynomial number of measurements. Section II B describes the algorithm for the compositional anzats optimization, which is followed by numerical results illustrating the efficiency and accuracy of the optimized ansatze for Cr₂ in seven different electronic states²³ and van der Waals complexes Ar–HCl(¹Σ) and Mg–NH(³Σ) in Section III. The work is summarized in Section IV.

II. THEORY

In VQE, a quantum computer calculates the expectation value $\langle\psi(\varphi)|\hat{H}|\psi(\varphi)\rangle$, which is minimized by varying φ to yield the lowest eigenvalue $E_{i=0}$ and an approximate representation of the corresponding eigenvector of \hat{H} . This method can be extended to compute excited states by optimizing²

$$\tilde{\varphi}_v = \operatorname{argmin}_{\varphi} \left[\langle\psi(\varphi)|\hat{H}|\psi(\varphi)\rangle + \sum_{i=0}^{v-1} \beta_i \langle\psi(\tilde{\varphi}_i)|\psi(\varphi)\rangle \right] \quad (1)$$

where $\beta_i \geq E_{i+1} - E_i$ and $\tilde{\varphi}_i$ denotes an optimal solution for the corresponding quantum state.

The quantum states $|\psi(\varphi)\rangle$ are obtained by quantum circuits acting on qubits and the Hamiltonian is expanded in quantum gates. Most generally,

$$\hat{H} = \sum_{i=0}^{4^n} A_i K_1^i \otimes K_2^i \dots \otimes K_n^i \quad (2)$$

where n is the number of qubits, $K_j^i \in \{\sigma_X, \sigma_Y, \sigma_Z, I\}$ acting on qubit j , $\{\sigma_i\}$ are the Pauli matrices, I is the identity matrix,

$$A_i = \frac{1}{2^n} \operatorname{Tr}[(K_1^i \otimes K_2^i \dots \otimes K_n^i) \cdot \mathbf{H}] \quad (3)$$

and \mathbf{H} is the Hamiltonian matrix in some basis. The computational complexity is determined by the number of non-zero terms in Eq. (2), which for a general matrix is 4^n ; and the complexity of the quantum circuits yielding $|\psi(\varphi)\rangle$. We begin by showing that the structure of DVR matrices allows an efficient quantum circuit representation of \hat{H} , scaling with n as $\operatorname{poly}(n)$.

A. Efficient measurement of DVR Hamiltonians

DVR is a finite basis representation, in which the coordinate operators (and consequently the potential energy) are diagonal. The DVR matrix of kinetic energy is not sparse. However, it has specific structure that is exploited here. We use DVR introduced

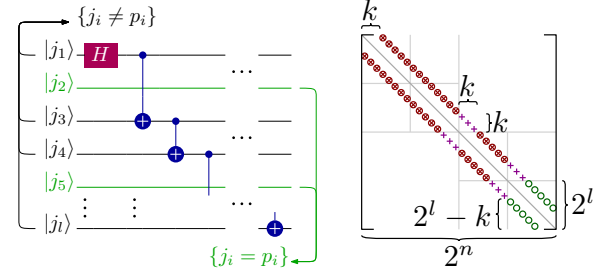


FIG. 1. Left: Preparation of state (10) from the computational basis. H denotes the Hadamard gate and the circles – the CNOT gates. Right: Measuring $t^{k[n]}$ that includes matrix elements on the main and k^{th} diagonals. The open circles \circ are obtained from projections of (10), \otimes – via $\mathbb{1}_2 \otimes t^{k[m]}$, and $+$ – by additional measurements in the entangled basis.

by Colbert and Miller²¹. Other DVR bases can be reduced to those in Ref.²¹ by coordinate transformations. As follows from Ref.²¹, the Hamiltonian matrix has the following structure:

$$H_{ij} = \begin{cases} d(i), & i = j, \\ f(|i - j|) + g(i + j), & i \neq j \end{cases} \quad (4)$$

We use a number encoding to map the DVR basis states onto qubit states, which allows VQE to compute the eigenvalues of \mathbf{H} of size $2^n \times 2^n$ using n qubits. It can be shown (see SM²⁴), that the functions f and g in Eq. (4) satisfy

$$\sum_{k=s}^{2^n-1} |f(k)| \leq O(s^{-\alpha}), \quad \alpha > 0, \quad (5)$$

$$\sum_{k=r}^{2^{n+1}-1} |g(k)| \leq O(r^{-\beta}), \quad \beta > 0, \quad (6)$$

for $1 \leq r \ll 2^n$ and $1 \leq s \ll 2^n$. Given a quantum state $|\psi\rangle$, our aim is to show that

$$\tau = \langle\psi|\hat{H}|\psi\rangle + O(\epsilon) \quad (7)$$

can be measured with the number of quantum circuits that scales polynomially with n and $1/\epsilon$. We seek to transform $|\psi\rangle$ by short-depth \hat{V}_i , so that

$$\tau = \sum_{i=1}^{\operatorname{poly}(n, 1/\epsilon)} \sum_{j=1}^{2^n} w_{ij} \left| \langle\psi|V_i^\dagger|j\rangle \right|^2 \quad (8)$$

where $|j\rangle$ is the state of n qubits in the computational Z basis.

We leverage the structure of the DVR matrix to decompose τ into contributions from a diagonal matrix (D), $s \approx \epsilon^{-1/\alpha}$ diagonal bands (t^k) and

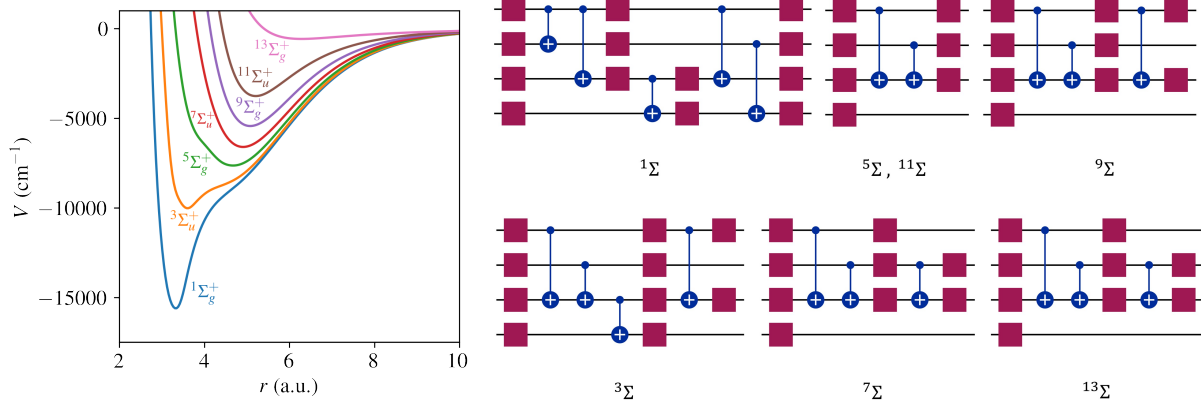


FIG. 2. Left: potential energy for Cr₂ from Ref.²³. Right: quantum circuits for VQE yielding the ground state energy with error $\leq 1 \text{ cm}^{-1}$. The squares represent the R_Y gates and the circles show the entangling CNOT gates.

$r \approx \epsilon^{-1/\beta}$ anti-diagonal components (a^k), as follows:

$$\tau = \langle D \rangle + \sum_{k=1}^{\lceil \epsilon^{-\frac{1}{\alpha}} \rceil} f(k) \langle t^{k[n]} \rangle + \sum_{k=1}^{\lceil \epsilon^{-\frac{1}{\beta}} \rceil} \left(g(k) \langle a^{k[n]} \rangle + g(2^n - k) \langle a^{(2^n - k)[n]} \rangle \right) + O(\epsilon).$$

The computation of the diagonal contribution $\langle D \rangle$ is classically efficient.

To construct $t^{k[n]}$, we note that $l \equiv \lceil \log_2(k+1) \rceil$ is the smallest number of qubits that allows k -th band. We consider l -qubit entangled states produced from the Z basis by a sequence of CNOT gates shown in Fig. 1 (left). The resulting state is

$$|+l\rangle = \frac{\bigotimes_i^l |j_i\rangle + \bigotimes_i^l |p_i\rangle}{\sqrt{2}}, \quad (10)$$

where j_i and p_i are single-qubit states, with at least one $j \neq p$. The projection of an n -qubit state onto the $|+l\rangle$ state has 2 non-zero off-diagonal matrix elements of magnitude 1/2. The binary representation of the row and column positions of these off-diagonal elements differ by l bits. The position of the non-zero off-diagonal elements is controlled by the position of the CNOT gates. Thus, the expectation value of $t^{k[l]}$ can be obtained by measurements with, at most, k l -qubit entangled states.

We now observe that $t^{k[m+1]} = \mathbb{1}_2 \otimes t^{k[m]} + \gamma$, where γ represents k pairs of elements missing from the middle of the tensor product matrix (pluses in Fig. 1 right). These elements can be directly targeted by additional measurements in the entangled basis constructed as described above for these specific elements, requiring at most k measurements if performed element-wise.

The full algorithm to compute $t^{k[n]}$ thus includes:

- (i) At most $2^l - k \leq k$ expectation values via circuits of depth $\leq l+1$ to obtain $t^{k[l]}$ (yielding elements represented by open circles in Fig. 1); (ii) Filling the gap (pluses in Fig. 1) in $\mathbb{1}_2 \otimes t^{k[m]}$ to produce $t^{k[m+1]}$, which requires measurements of at most k projections on entangled states via circuits of depth at most $\lceil \log_2 2k \rceil$; (iii) A total of $n-l$ iterations to fill the entire band. The total number of measurement circuits for $t^{k[n]}$ is thus

$$\text{Comp} \left(t^{k[n]} \right) < (n+1 - \log_2 k) k. \quad (11)$$

To construct the anti-diagonals $a^{k[n]}$, we first note that the expectation values of $a^{1[1]} = \begin{bmatrix} 1 & 0 \\ 0 & 0 \end{bmatrix}$, $a^{2[1]} = \begin{bmatrix} 0 & 1 \\ 1 & 0 \end{bmatrix}$ and $a^{3[1]} = \begin{bmatrix} 0 & 0 \\ 0 & 1 \end{bmatrix}$ can be obtained by sampling one-qubit measurements of ψ in Z to get $\langle a^{1[1]} \rangle_\psi$ and $\langle a^{3[1]} \rangle_\psi$ and in X to get $\langle a^{2[1]} \rangle_\psi$. The elements $a^{k[m+1]}$ can be obtained by combining $\mathbb{1}_2 \otimes a^{k[m]}$ and $a^{k[m]} \otimes \mathbb{1}_2$, which at most doubles the number of measurements²⁴.

We limit the construction to $r = \log_2 \epsilon/\beta$ anti-diagonals. Eq. (6) ensures that the remaining anti-diagonals will contribute less than ϵ to the expectation value (9). The circuits can be constructed from $a^{k[1]}$ by incrementally increasing the number of qubits to $a^{k[r]}$, which requires $\leq 2^r$ bases in total. The contributions from the anti-diagonals are obtained by measuring $n-r$ qubits in the computational basis and $a^{k[r]}$ thus constructed. For the $n-s$ qubits, one needs to take into account only the all- \uparrow and all- \downarrow outputs, yielding the up-most and down-most 2^r anti-diagonals. The total number of bases for this protocol is bounded by

$$2^r < 2^{1 - \frac{\log_2 \epsilon}{\beta}} = 2\epsilon^{-\frac{1}{\beta}}. \quad (12)$$

Electronic state	v	BM	E_v^{VQE}		
			\mathcal{C}_1	$\mathcal{C}_{0.01}$	Linear
$^1\Sigma_g^+$	0	-15358.94	-15358.87	-15358.99	-15358.99
	1	-14846.67	-14838.70	-14846.75	-14846.96
	2	-14333.21	-14310.29	-14332.80	-14332.82
	3	-13826.93	-13797.65	-13826.87	-13827.29
	4	-13334.02	-13275.12	-13318.77	-13335.45
$^3\Sigma_u^+$	0	-9862.07	-9861.37	-9862.14	-9862.14
	1	-9559.46	-9538.97	-9556.67	-9559.41
	2	-9300.92	-9240.74	-9266.82	-9300.88
	3	-9080.60	-9068.09	-9079.26	-9085.40
	4	-8897.58	-8866.09	-8870.57	-8896.82
$^5\Sigma_g^+$	0	-7566.53	-7565.88	-7566.50	-7566.50
	1	-7416.28	-7397.28	-7416.28	-7416.29
	2	-7264.92	-7181.98	-7264.60	-7264.69
	3	-7114.40	-7075.88	-7117.83	-7118.43
	4	-6965.91	-7001.98	-6953.74	-6958.08
$^7\Sigma_u^+$	0	-6519.01	-6519.04	-6519.04	
	1	-6350.36	-6350.11	-6350.11	
	2	-6183.38	-6185.17	-6185.17	
	3	-6018.09	-6018.12	-6018.28	
	4	-5854.50	-5848.69	-5849.10	
$^9\Sigma_g^+$	0	-5348.79	-5348.82	-5348.82	
	1	-5175.81	-5175.51	-5175.51	
	2	-5005.17	-5008.55	-5008.56	
	3	-4836.85	-4829.80	-4829.92	
	4	-4670.91	-4683.42	-4683.68	
$^{11}\Sigma_u^+$	0	-3677.68	-3677.00	-3677.68	-3677.68
	1	-3507.89	-3489.51	-3507.82	-3507.82
	2	-3341.77	-3253.24	-3341.26	-3341.40
	3	-3180.16	-3133.59	-3185.51	-3186.93
	4	-3023.07	-3061.61	-3001.04	-3012.82
$^{13}\Sigma_g^+$	0	-548.68	-548.65	-548.67	-548.68
	1	-497.16	-496.47	-496.84	-497.15
	2	-449.18	-443.48	-448.36	-449.26
	3	-404.71	-382.88	-390.96	-404.67
	4	-363.58	-369.09	-360.62	-362.99
	5	-325.67	-315.46	-310.29	-325.72

TABLE I. Vibrational energy (in cm^{-1}) of Cr_2 ($v = 0 - 5$) in different electronic states. The benchmark (BM) results are obtained with a converged DVR basis. VQE uses quantum circuits shown in Fig. 2. An extended table for a wider range of molecular states is in SM²⁴.

B. Numerical ansatz optimization

In this section, we demonstrate that DVR Hamiltonians also lead to very efficient quantum ansatze

for representing ro-vibrational states of molecules by states of a quantum computer. In order to apply VQE, it is necessary to find a proper ansatz for $|\psi\rangle$. It is not always clear how to select the ansatz for $|\psi\rangle$. Previous work on electronic structure proposed various types of ansatzes for VQE with both fixed^{3,7,25–29} and adaptive structure^{30–39}. Unlike electronic structure problems, where interactions are pairwise additive, ro-vibrational energy calculations are determined by a wide range of potential energy landscapes, which are highly molecule-specific. In order to obtain the most efficient quantum circuit representations of $|\psi\rangle$ for VQE with DVR matrices, we develop and illustrate an iterative algorithm for ansatz construction that minimizes the number of entangling gates for each specific molecule. This algorithm is inspired by work in Refs.^{40–42}.

Our starting point is⁷:

$$|\psi(\varphi)\rangle = \prod_{d=0}^{k-1} \left[\prod_{q=0}^{n-1} U^{q,d}(\varphi_d^q) \times U_{\text{ent}}^d \right] \times \prod_{q=0}^{N-1} U^{q,k}(\varphi_k^q) |0^n\rangle, \quad (13)$$

where $U^{q,d}(\varphi)$ represent $R_Y = \exp(-i\varphi\sigma_Y/2)$ for qubit q , and k is the number of repetitions of the ansatz blocks. The form of U_{ent}^d is determined by the ansatz optimization algorithm described below. For reference, we also use

$$U_{\text{ent}} = \prod_{q=0}^{n-1} \text{CNOT}(q, q+1), \quad (14)$$

denoted hereafter as linear to reflect the position of CNOT with q .

Our algorithm starts with a non-entangled quantum state given by Eq. (13) with a predetermined number of blocks k and U_{ent} set to identity. The method considers $\text{CNOT}(q, p) \forall q < p$ as candidate gates for U_{ent}^d , with each d segment treated independently. In each optimization step, the candidate gate that lowers the VQE energy is added without replacement until convergence. Here, we aim to converge the VQE calculation of the ground state either to 1 cm^{-1} or 0.01 cm^{-1} , which yields quantum circuits of different complexity denoted \mathcal{C}_1 and $\mathcal{C}_{0.01}$. This convergence error is with respect to the lowest eigenstate of the DVR matrix with the same number of DVR bases.

III. NUMERICAL RESULTS

We calculate the ro-vibrational energy levels of diatomic (Cr_2) and triatomic ($\text{Ar}-\text{HCl}$ and $\text{Mg}-\text{NH}$)

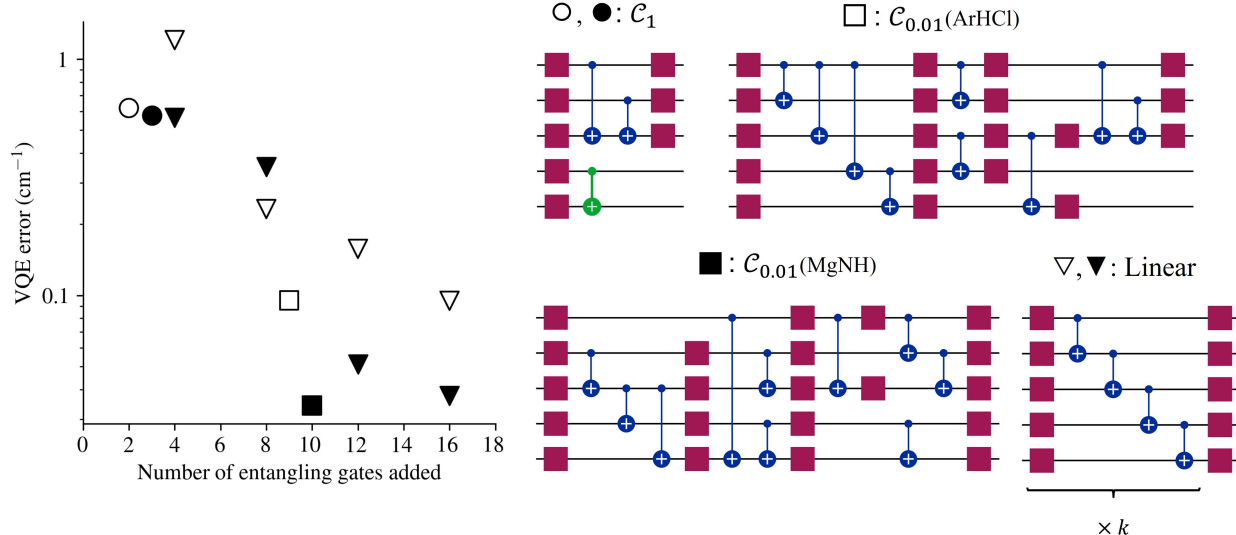


FIG. 3. Left: VQE error for lowest energy of Ar–HCl (open symbols) and Mg–NH (full symbols) computed with optimized quantum circuits in the right panel. Circles – with \mathcal{C}_1 circuits; squares – with $\mathcal{C}_{0.01}$ circuits; triangles – with ansatz (13) using (left to right) $k = 1, 2, 3$ and 4 and Eq. (14). The \mathcal{C}_1 ansatz for Mg – NH excludes the gate shown in green.

Molecule	v	E_v (experiment)	E_v (computed in ⁴³)	E_v (classical, present)	E_v (VQE)		
					\mathcal{C}_1	$\mathcal{C}_{0.01}$	Linear
ArHCl	0	-114.7 ⁴⁴	-115.151	-115.265	-114.645	-115.169	-115.171
	1	-91.04 ^{45,46}	-91.485	-91.642	-80.824	-90.485	-90.929
	2	-82.26 ⁴⁷	-82.717	-82.825	-75.900	-82.986	-82.650
MgNH	0	-	-	-88.227	-87.650	-88.191	-88.190
	1	-	-	-63.603	-56.050	-62.730	-62.664
	2	-	-	-55.461	-55.145	-54.850	-54.866

TABLE II. Vibrational energy (in cm^{-1}) of Ar–HCl and Mg–NH by VQE with 32 DVR points and 5-qubit circuits.

systems. For diatomic molecules we use the DVR Hamiltonian from Ref.²¹. For triatomic complexes, we use the DVR approach by Choi and Light²². We benchmark the VQE results by the vibrational levels calculated using direct diagonalization with the converged DVR basis and previous literature results, where available.

Table I (extended version in the SM²⁴) demonstrates VQE for vibrational states $v = 0 - 5$ of seven electronic states of Cr_2 with zero rotational angular momentum. We use the interaction potentials from Ref.²³, illustrated in Fig. 2. The VQE calculations use 16 DVR points placed to span the range including the minimum of the potential energy. The Hamiltonian is represented by the expansion (2) including ≈ 130 Pauli terms. Table I displays VQE results obtained with three types of quantum circuits: the linear ansatz (14) with 3 repetitions, and optimized circuits \mathcal{C}_1 (shown in Fig. 2) and $\mathcal{C}_{0.01}$

(shown in the SM²⁴).

For tri-atomic complexes, we use either 32 or 64 DVR basis states and accurate atom - molecule potential energy surfaces by Hutson for Ar–HCl⁴³ and by Soldán et al. for Mg–NH⁴⁸. We keep both HCl and NH in the ground ro-vibrational state and compute the vibrational states supported by the atom - molecule interaction potential. We obtain the DVR points for the triatomic systems by diagonalizing the coordinate representations. The parameters to generate the DVR points are selected to cover the low-energy regions of the potential energy surface. The 32-point DVR Hamiltonians are represented by 165 (Ar–HCl) and 170 (Mg–NH) Pauli terms in Eq. (2) acting on 5 qubits, while the 64-point DVR Hamiltonians are represented by 610 (Ar–HCl) and 621 (Mg–NH) Pauli terms (2) acting on 6 qubits. As above, we construct three types of quantum circuits: \mathcal{C}_1 , $\mathcal{C}_{0.01}$ and the linear ansatz (14) with k repetitions.

Figure 3 and Table II show that accurate results can be obtained with very shallow circuits.

IV. SUMMARY

In conclusion, we have presented two significant results. First, we have shown that the structure of DVR matrices can be leveraged to represent molecular Hamiltonians by the polynomial (in the number of qubits n) number of quantum circuits. Second, we have demonstrated that DVR leads to efficient quantum circuits for VQE computations of ro-vibrational energy levels. To show this, we have introduced a general approach to constructing the quantum ansatz by combining DVR with VQE and a greedy search of gate sequences. The results yield compact representations of vibrational states by quantum circuits of a gate-based quantum computer. We have shown that both the ground and excited vibrational energies can be computed with the relative accuracy of $< 1\%$ using very simple, in some cases, partially entangled circuits. The accuracy of 1 cm^{-1} can be achieved with < 20 (< 5 entangling) gates and 4 qubits for diatomic molecules and < 30 (< 9 entangling) gates with 5 qubits for triatomic van der Waals complexes. This should be compared with previous VQE calculations of ro-vibrational energy levels that required extended quantum circuits with > 200 (for CO, COH and O₃ molecules¹⁷) or between 44 and 140 292 (for CO₂, H₂CO and HCOOH molecules¹⁶) entangling gates. We note that DVR does not require global fits of potential energy surfaces or integrals over the potential energy for the construction of the Hamiltonian matrix. The implementation of VQE with DVR in first quantization does not require normal-mode analysis for the construction of the quantum ansatz. The present approach can be readily extended beyond molecular dynamics. For example, this method can be directly applied to designing efficient quantum circuits for variational computations of the eigenspectra of semiconductor quantum dots⁴⁹.

V. SUPPLEMENTARY MATERIAL

The supplemental material²⁴ includes Sections 1 – 3. Section 1 provides detailed proofs that support Eqs. (5) and (6) of the main text. Sections 2 is a detailed description of the quantum measurement algorithms, including a summary of the measurement complexity. Section 3 presents the quantum circuits and optimization details for the numerical computations.

VI. ACKNOWLEDGMENTS

This work was support by NSERC of Canada and the Stewart Blusson Quantum Matter Institute.

VII. CONFLICT OF INTEREST STATEMENT

The authors have no conflicts to disclose.

VIII. AUTHOR CONTRIBUTIONS STATEMENT

All authors have designed the concept of this work and co-wrote the manuscript. The algorithm presented in Section II A was developed by DB. The algorithm for ansatz optimization was developed by KA and RVK and the numerical calculations were performed by KA.

IX. DATA AVAILABILITY STATEMENT

The data that support the findings of this study are available within the article and its supplementary material.

- ¹J. Tilly, H. Chen, S. Cao, D. Picozzi, K. Setia, Y. Li, E. Grant, L. Woessig, I. Rungger, G. H. Booth, and J. Tenneyson, “The variational quantum eigensolver: a review of methods and best practices,” (2021), arXiv:2111.05176.
- ²O. Higgott, D. Wang, and S. Brierley, “Variational Quantum Computation of Excited States,” *Quantum* **3**, 156 (2019).
- ³A. Peruzzo, J. McClean, P. Shadbolt, M.-H. Yung, X.-Q. Zhou, P. J. Love, A. Aspuru-Guzik, and J. L. O’Brien, “A variational eigenvalue solver on a photonic quantum processor,” *Nat. Commun.* **5**, 4213 (2014).
- ⁴J. R. McClean, J. Romero, R. Babbush, and A. Aspuru-Guzik, “The theory of variational hybrid quantum-classical algorithms,” *New J. Phys.* **18**, 023023 (2016).
- ⁵P. J. O’Malley, R. Babbush, I. D. Kivlichan, J. Romero, J. R. McClean, R. Barends, J. Kelly, P. Roushan, A. Tranter, N. Ding, B. Campbell, Y. Chen, Z. Chen, B. Chiaro, A. Dunsworth, A. G. Fowler, E. Jeffrey, E. Lucero, A. Megrant, J. Y. Mutus, M. Neeley, C. Neill, C. Quintana, D. Sank, A. Vainsencher, J. Wenner, T. C. White, P. V. Coveney, P. J. Love, H. Neven, A. Aspuru-Guzik, and J. M. Martinis, “Scalable quantum simulation of molecular energies,” *Phys. Rev. X* **6**, 031007 (2016).
- ⁶Y. Shen, X. Zhang, S. Zhang, J.-N. Zhang, M.-H. Yung, and K. Kim, “Quantum implementation of the unitary coupled cluster for simulating molecular electronic structure,” *Phys. Rev. A* **95**, 020501 (2017).
- ⁷A. Kandala, A. Mezzacapo, K. Temme, M. Takita, M. Brink, J. M. Chow, and J. M. Gambetta, “Hardware-efficient variational quantum eigensolver for small molecules and quantum magnets,” *Nature* **549**, 242–246 (2017).
- ⁸J. I. Colless, V. V. Ramasesh, D. Dahmen, M. S. Blok, M. E. Kimchi-Schwartz, J. R. McClean, J. Carter, W. A. de Jong, and I. Siddiqi, “Computation of molecular spectra on a

quantum processor with an error-resilient algorithm," *Phys. Rev. X* **8**, 011021 (2018).

⁹C. Hempel, C. Maier, J. Romero, J. McClean, T. Monz, H. Shen, P. Jurcevic, B. P. Lanyon, P. Love, R. Babbush, A. Aspuru-Guzik, R. Blatt, and C. F. Roos, "Quantum chemistry calculations on a trapped-ion quantum simulator," *Phys. Rev. X* **8**, 031022 (2018).

¹⁰Y. Nam, J.-S. Chen, N. C. Pisenti, K. Wright, C. Delaney, D. Maslov, K. R. Brown, S. Allen, J. M. Amini, J. Apisdorf, K. M. Beck, A. Blinov, V. Chaplin, M. Chmielewski, C. Collins, S. Debnath, A. M. Ducore, K. M. Hudek, M. Keesan, S. M. Kreikemeier, J. Mizrahi, P. Solomon, M. Williams, J. D. Wong-Campos, C. Monroe, and J. Kim, "Ground-state energy estimation of the water molecule on a trapped ion quantum computer," (2019), arXiv:1902.10171.

¹¹S. McArdle, S. Endo, A. Aspuru-Guzik, S. C. Benjamin, and X. Yuan, "Quantum computational chemistry," *Rev. Mod. Phys.* **92**, 015003 (2020).

¹²C. Kokail, C. Maier, R. van Bijnen, T. Brydges, M. K. Joshi, P. Jurcevic, C. A. Muschik, P. Silvi, R. Blatt, C. F. Roos, and P. Zoller, "Self-verifying variational quantum simulation of lattice models," *Nature* **569**, 355–360 (2019).

¹³C.-K. Lee, C.-Y. Hsieh, S. Zhang, and L. Shi, "Variational quantum simulation of chemical dynamics with quantum computers," *J. Chem. Theory Comput.* **18**, 2105–2113 (2022).

¹⁴J. Apanavicius, Y. Feng, Y. Flores, M. Hassan, and M. McGuigan, "Morse potential on a quantum computer for molecules and supersymmetric quantum mechanics," (2021), arXiv:2102.05102.

¹⁵S. McArdle, A. Mayorov, X. Shan, S. Benjamin, and X. Yuan, "Digital quantum simulation of molecular vibrations," *Chem. Sci.* **10**, 5725–5735 (2019).

¹⁶P. J. Ollitrault, A. Baiardi, M. Reiher, and I. Tavernelli, "Hardware efficient quantum algorithms for vibrational structure calculations," *Chem. Sci.* **11**, 6842–6855 (2020).

¹⁷N. P. D. Sawaya, F. Paesani, and D. P. Tabor, "Near- and long-term quantum algorithmic approaches for vibrational spectroscopy," *Phys. Rev. A* **104**, 062419 (2021).

¹⁸E. Lötstedt, K. Yamanouchi, and Y. Tachikawa, "Evaluation of vibrational energies and wave functions of CO₂ on a quantum computer," *AVS Quantum Sci.* **4**, 036801 (2022).

¹⁹E. Lötstedt, K. Yamanouchi, T. Tsuchiya, and Y. Tachikawa, "Calculation of vibrational eigenenergies on a quantum computer: Application to the fermi resonance in CO₂," *Phys. Rev. A* **103**, 062609 (2021).

²⁰M. T. Nguyen, Y.-L. Lee, D. Alfonso, Q. Shao, and Y. Duan, "Description of reaction and vibrational energetics of CO₂–NH₃ interaction using quantum computing algorithms," *AVS Quantum Science* **5**, 013801 (2023).

²¹D. T. Colbert and W. H. Miller, "A novel discrete variable representation for quantum mechanical reactive scattering via the s-matrix kohn method," *J. Chem. Phys.* **96**, 1982–1991 (1992).

²²S. E. Choi and J. C. Light, "Determination of the bound and quasibound states of Ar–HCl van der waals complex: Discrete variable representation method," *J. Chem. Phys.* **92**, 2129–2145 (1990).

²³Z. Pavlović, R. V. Krems, R. Côté, and H. R. Sadeghpour, "Magnetic feshbach resonances and zeeman relaxation in bosonic chromium gas with anisotropic interaction," *Phys. Rev. A* **71**, 061402 (2005).

²⁴"Supplementary materials,".

²⁵J. Romero, R. Babbush, J. R. McClean, C. Hempel, P. J. Love, and A. Aspuru-Guzik, "Strategies for quantum computing molecular energies using the unitary coupled cluster ansatz," *Quantum Sci. Technol.* **4**, 014008 (2018).

²⁶D. Wecker, M. B. Hastings, and M. Troyer, "Progress towards practical quantum variational algorithms," *Phys. Rev. A* **92**, 042303 (2015).

²⁷J. Lee, W. J. Huggins, M. Head-Gordon, and K. B. Whaley, "Generalized unitary coupled cluster wave functions for quantum computation," *J. Chem. Theory Comput.* **15**, 311–324 (2019).

²⁸P. K. Barkoutsos, J. F. Gonthier, I. Sokolov, N. Moll, G. Salis, A. Fuhrer, M. Ganzhorn, D. J. Egger, M. Troyer, A. Mezzacapo, S. Filipp, and I. Tavernelli, "Quantum algorithms for electronic structure calculations: Particle-hole hamiltonian and optimized wave-function expansions," *Phys. Rev. A* **98**, 022322 (2018).

²⁹R. Wiersema, C. Zhou, Y. de Sereville, J. F. Carrasquilla, Y. B. Kim, and H. Yuen, "Exploring entanglement and optimization within the hamiltonian variational ansatz," *PRX Quantum* **1**, 020319 (2020).

³⁰H. R. Grimsley, S. E. Economou, E. Barnes, and N. J. Mayhall, "An adaptive variational algorithm for exact molecular simulations on a quantum computer," *Nat. Commun.* **10**, 3007 (2019).

³¹A. M. Romero, J. Engel, H. L. Tang, and S. E. Economou, "Solving nuclear structure problems with the adaptive variational quantum algorithm," *Phys. Rev. C* **105**, 064317 (2022).

³²H. L. Tang, V. Shkolnikov, G. S. Barron, H. R. Grimsley, N. J. Mayhall, E. Barnes, and S. E. Economou, "Qubit-ADAPT-VQE: An adaptive algorithm for constructing hardware-efficient ansätze on a quantum processor," *PRX Quantum* **2**, 020310 (2021).

³³I. G. Ryabinkin, R. A. Lang, S. N. Genin, and A. F. Izmaylov, "Iterative qubit coupled cluster approach with efficient screening of generators," *J. Chem. Theory Comput.* **16**, 1055–1063 (2020).

³⁴Y. Zhang, L. Cincio, C. F. A. Negre, P. Czarnik, P. J. Coles, P. M. Anisimov, S. M. Mniszewski, S. Tretiak, and P. A. Dub, "Variational quantum eigensolver with reduced circuit complexity," *npj Quantum Information* **8**, 96 (2022).

³⁵M. Ostaszewski, E. Grant, and M. Benedetti, "Structure optimization for parameterized quantum circuits," *Quantum* **5**, 391 (2021).

³⁶M. Bilkis, M. Cerezo, G. Verdon, P. J. Coles, and L. Cincio, "A semi-agnostic ansatz with variable structure for variational quantum algorithms," *Quantum Mach. Intell.* **5**, 43 (2023).

³⁷A. G. Rattew, S. Hu, M. Pistoia, R. Chen, and S. Wood, "A domain-agnostic, noise-resistant, hardware-efficient evolutionary variational quantum eigensolver," (2020), arXiv:1910.09694.

³⁸D. Chivilikhin, A. Samarin, V. Ulyantsev, I. Iorsh, A. R. Oganov, and O. Kyriienko, "Mog-vqe: Multiobjective genetic variational quantum eigensolver," (2020), arXiv:2007.04424.

³⁹Y. Du, T. Huang, S. You, M.-H. Hsieh, and D. Tao, "Quantum circuit architecture search for variational quantum algorithms," *npj Quantum Inf.* **8**, 62 (2022).

⁴⁰H. R. Grimsley, S. E. Economou, E. Barnes, and N. J. Mayhall, "An adaptive variational algorithm for exact molecular simulations on a quantum computer," *Nat. Commun.* **10**, 3007 (2019).

⁴¹E. Torabian and R. V. Krems, "Compositional optimization of quantum circuits for quantum kernels of support vector machines," *Phys. Rev. Res.* **5**, 013211 (2023).

⁴²X. Guo, J. Dai, and R. V. Krems, "Benchmarking of quantum fidelity kernels for gaussian process regression," *Mach. Learn.: Sci. Technol.* **5**, 035081 (2024).

⁴³J. M. Hutson, "Vibrational dependence of the anisotropic intermolecular potential of argon-hydrogen chloride," *J.*

Phys. Chem. **96**, 4237–4247 (1992).

⁴⁴A. S. Pine and B. J. Howard, “Hydrogen bond energies of the HF and HCl dimers from absolute infrared intensities,” J. Chem. Phys. **84**, 590–596 (1986).

⁴⁵K. L. Busarow, G. A. Blake, K. Laughlin, R. Cohen, Y. Lee, and R. Saykally, “Tunable far-infrared laser spectroscopy in a planar supersonic jet: The σ bending vibration of Ar³⁵HCl,” Chem. Phys. Lett. **141**, 289–291 (1987).

⁴⁶R. L. Robinson, D.-H. Gwo, and R. J. Saykally, “Far infrared laser stark spectroscopy of the σ bending vibration of ArHCl,” Mol. Phys. **63**, 1021–1029 (1988).

⁴⁷R. L. Robinson, D. Gwo, and R. J. Saykally, “The high-resolution far infrared spectrum of a van der waals stretching vibration: The ν_3 band of ar–hcl,” J. Chem. Phys. **87**, 5156–5160 (1987).

⁴⁸P. Soldán, P. S. Žuchowski, and J. M. Hutson, “Prospects for sympathetic cooling of polar molecules: NH with alkali-metal and alkaline-earth atoms – a new hope,” Faraday Discuss. **142**, 191–201 (2009).

⁴⁹Y. Wang, J. P. Dehollain, F. Liu, U. Mukhopadhyay, M. S. Rudner, L. M. K. Vandersypen, and E. Demler, “Ab initio exact diagonalization simulation of the nagaoka transition in quantum dots,” Phys. Rev. B **100**, 155133 (2019).

Supplemental Material for “Variational quantum computation of vibrational energy using discrete variable representation”

K. Asnaashari, D. Bondarenko, and R. V. Krems
*Department of Chemistry, University of British Columbia,
Vancouver, B.C. V6T 1Z1, Canada*
*Stewart Blusson Quantum Matter Institute,
Vancouver, B.C. V6T 1Z4, Canada*
(Dated: October 15, 2024)

This supplemental material includes Sections 1 – 3. Section 1 provides detailed proofs that support Eqs. (5) and (6) of the main text. Sections 2 is a detailed description of the quantum measurement algorithms, including a summary of the measurement complexity. Section 3 presents the quantum circuits and optimization details for the numerical computations.

1. DECAY OF OFF-DIAGONAL MATRIX ELEMENTS

We consider a discrete variable representation (DVR) introduced by Colbert and Miller [1] with N basis states. As mentioned in the main text, we use a number encoding to map the DVR basis states onto the qubit states, which allows VQE to compute the eigenvalues of the Hamiltonian matrix of size $2^n \times 2^n$ using n qubits. Thus, $N = 2^n$.

The kinetic energy operator in the DVR basis for a particle with mass m on a grid of $x = [a, b]$ with the uniform spacing Δx has the matrix elements [1]:

$$T_{ij} = \frac{\hbar^2}{2m\Delta x^2} \times \begin{cases} d(i) & i = j, \\ f(|i - j|) + g(i + j), & i \neq j. \end{cases} \quad (S1)$$

Our first goal is to show that

$$\sum_{k=s}^{2^n-1} |f(k)| \leq O(s^{-\alpha}), \quad \alpha > 0, \quad (S2)$$

$$\sum_{k=r}^{2^{n+1}-1} |g(k)| \leq O(r^{-\beta}), \quad \beta > 0, \quad (S3)$$

where $r \ll N$ and $s \ll N$, and N is assumed to be large.

A. Expansion in Fourier functions

Consider an equally-spaced 1D grid with endpoints a and b

$$x_j = b + j\Delta x, \quad \Delta x = \frac{b - a}{N}, \quad j = 1, \dots, N - 1. \quad (S4)$$

Given an orthonormal basis $\{\phi_n\}$, the matrix elements of the kinetic energy can be written as

$$T_{ij} = -\frac{\hbar^2}{2m}\Delta x \sum_{n=0}^{N-1} \phi_n(x_i)\phi_n''(x_j). \quad (S5)$$

For the boundary conditions $\phi_n(x_0 \equiv a) = \phi_n(x_N \equiv b) = 0$, the associated Fourier functions are

$$\phi_n(x) = \left(\frac{2}{b - a} \right)^{1/2} \sin \left[\frac{n\pi(x - a)}{b - a} \right]. \quad (S6)$$

For this basis, the sum can be evaluated analytically yielding [1]

$$T_{ij} = \begin{cases} \frac{\hbar^2}{2m} \frac{1}{(b-a)^2} \frac{\pi^2}{2} \left[\frac{2N^2+1}{3} - \frac{1}{\sin^2(\pi j/N)} \right], & i = j, \\ \frac{\hbar^2}{2m} \frac{(-1)^{i-j}}{(b-a)^2} \frac{\pi^2}{2} \left\{ \frac{1}{\sin^2[\pi(i-j)/2N]} - \frac{1}{\sin^2[\pi(i+j)/2N]} \right\}, & i \neq j. \end{cases} \quad (S7)$$

Following Colbert and Miller, we now consider the cases of infinite lattices, relevant for radial molecular coordinates, and a case of finite a and b .

1. Infinite lattice [$a = -\infty, b = \infty$]

The finite grid spacing $\Delta x = \frac{b-a}{N}$ requires $N \rightarrow \infty$. Eq. (S7) becomes

$$T_{ij} = \frac{\hbar^2}{2m\Delta x^2} (-1)^{i-j} \begin{cases} \frac{\pi^2}{3}, & i = j, \\ \frac{2}{(i-j)^2}, & i \neq j. \end{cases} \quad (\text{S8})$$

Note that in this case $g(i+j)$ vanishes. It is easy to see that

$$|f(k)| = \frac{2}{(i-j)^2} \quad (\text{S9})$$

satisfies Eq. (S2). To prove this, we note that for functions that are (strictly) monotonically decaying in absolute value

$$\int_s^u |f(k)| dk < \sum_{k=s}^u |f(k)| < \int_{s-1}^{u-1} |f(k)| dk. \quad (\text{S10})$$

For our choice of $f(\cdot)$ this yields the bound

$$\sum_{k=s}^{2^n-1} |f(k)| < 2 \int_{s-1}^{2^n-2} \frac{dk}{k^2} = 2 \left(\frac{1}{s-1} - \frac{1}{2^n-2} \right) < 3s^{-1}. \quad (\text{S11})$$

2. Infinite lattice [$a = 0, b = \infty$]

For the lattice with $[a = 0, b = \infty]$, the matrix elements

$$T_{ij} = \frac{\hbar^2}{2m\Delta x^2} (-1)^{i-j} \begin{cases} \frac{\pi^2}{3} - \frac{1}{2i^2}, & i = j, \\ \frac{2}{(i-j)^2} - \frac{2}{(i+j)^2}, & i \neq j. \end{cases} \quad (\text{S12})$$

include $g(k)$. Since Eq. (S11) applies to $g(k)$, the arguments in Subsubsection (1 A 1) apply to Eq. (12).

3. Finite lattice [a, b]

Observe that the prefactor in Eq. (S7) satisfy $\frac{\hbar^2}{2m} \frac{1}{(b-a)^2} \frac{\pi^2}{2} \cdot \frac{2m\Delta x^2}{\hbar^2} = \frac{\pi^2}{2N^2}$. Consider the following functions

$$|\tilde{f}(k)| = \frac{\pi^2}{2N^2} \left[\frac{1}{\sin^2(\pi k/2N)} - 1 \right], \quad (\text{S13})$$

$$|\tilde{g}(k)| = \frac{\pi^2}{2N^2} \left[\frac{1}{\sin^2(\pi k/2N)} - 1 \right]. \quad (\text{S14})$$

Eq. (S10) yields

$$\sum_{k=s}^{N-1} \frac{1}{\sin^2(\pi k/2N)} = \frac{2N}{\pi} \sum_{k=s} \frac{\pi}{2N} \frac{1}{\sin^2(\pi k/2N)} \quad (\text{S15})$$

$$< \frac{2N}{\pi} \int_{\frac{\pi(s-1)}{2N}}^{\frac{\pi}{2}} \frac{dx}{\sin^2(x)} \quad (\text{S16})$$

$$= \frac{2N}{\pi} \cot \left[\frac{\pi(s-1)}{2N} \right] \quad (\text{S17})$$

Using the Laurent series for $\cot(y)$ around $y = 0$, we can write

$$\frac{2N}{\pi} \cot \left[\frac{\pi(s-1)}{2N} \right] = \frac{4N^2}{\pi^2(s-1)} - \frac{(s-1)}{3} + O\left(\frac{s^3}{N^2}\right). \quad (\text{S18})$$

This yields

$$\sum_{k=s}^{2^n-1} |\tilde{f}(k)| < \frac{\pi^2}{2N^2} \left[\frac{4N^2}{\pi^2(s-1)} - \frac{(s-1)}{3} - (N-1-s) + O\left(\frac{s^3}{N^2}\right) \right] \quad (\text{S19})$$

$$< \frac{2}{s-1} + O\left(\frac{s^3}{N^4}\right) \quad (\text{S20})$$

$$< 3s^{-1}. \quad (\text{S21})$$

For $g(k)$, we exploit the symmetry of $\sin(\cdot)$ to write

$$\sum_{k=r}^{2^{n+1}-1-r} \frac{1}{\sin^2(\pi k/2N)} = 1 + 2 \sum_{k=r}^{2^n-1} \frac{1}{\sin^2(\pi k/2N)}, \quad (\text{S22})$$

and apply Eqs. (19)-(21).

2. QUANTUM MEASUREMENT OF THE KINETIC ENERGY

Given a quantum state $|\psi\rangle$ prepared by a quantum computer, our aim is to show that

$$\tau = \langle \psi | \hat{H} | \psi \rangle + O(\epsilon) \quad (\text{S23})$$

can be measured with the number of quantum circuits that scales polynomially with n and $1/\epsilon$. We seek to transform $|\psi\rangle$ by short-depth \hat{V}_i , so that

$$\tau = \sum_{i=1}^{\text{poly}(n, 1/\epsilon)} \sum_{j=1}^{2^n} w_{ij} \left| \langle \psi | V_i^\dagger | j \rangle \right|^2 \quad (\text{S24})$$

where $|j\rangle$ is the state of n qubits in the computational Z basis.

A. DVR matrix truncation

The results of Section 1 suggest that it is possible to truncate the DVR matrix of the kinetic energy as follows:

$$T_{ij}^{(s,r)} = \frac{\hbar^2}{2m\Delta x^2} \times \begin{cases} d(i) & i = j, \\ f(|i-j|) + g(i+j) & i \neq j, |i-j| < s, i+j < r, \\ 0 & \text{otherwise.} \end{cases} \quad (\text{S25})$$

We now aim to determine the values of s and r such that $\langle \psi | T | \psi \rangle = \langle \psi | T^{(s,r)} | \psi \rangle + O(\epsilon)$.

Consider a k^{th} (anti)-diagonal matrix

$$K_{ij}^{k\pm\pm} \equiv \delta_{i\pm j, \pm k}, \quad (\text{S26})$$

where only $++$, $+-$ and $--$ combination of signs are used. It is straightforward to check that $\|K\psi\|_2 \leq \|\psi\|_2$ (and the inequality is tight). The Cauchy–Schwarz inequality $|\langle \psi, K\psi \rangle| \leq \|\psi\|_2 \|K\psi\|_2$ yields the bound for the expectation value of K

$$|\langle \psi, K\psi \rangle| \leq \|\psi\|_2^2. \quad (\text{S27})$$

Due to the triangle inequality, for $\|\psi\|_2^2 = 1$, the approximation error is bounded by

$$\begin{aligned} \left| \langle \psi | (T - T^{(s,r)}) | \psi \rangle \right| &= \left| \langle \psi | \left(\sum_{k=s}^{2^n-1} f(k) [K^{k-+} + K^{k--}] + \sum_{k=r}^{2^{n+1}-1} g(k) K^{k++} \right) | \psi \rangle \right| \\ &\leq E(T) \cdot \left(2 \sum_{k=s}^{2^n-1} |f(k)| + \sum_{k=r}^{2^{n+1}-1} |g(k)| \right) \\ &\leq E(T) \cdot [2O(s^{-\alpha}) + O(r^{-\beta})], \end{aligned} \quad (\text{S28})$$

where $E(T) = \hbar^2 [2m\Delta x^2]^{-1}$. Due to Eqs. (S2)-(S3) for $f(\cdot)$ and $g(\cdot)$, $T^{(s,r)}$ is a good approximation of T for $s \sim \epsilon^{-\frac{1}{\alpha}}$ and $r \sim \epsilon^{-\frac{1}{\beta}}$.

B. Measuring the expectation value of the truncated operator $T^{(s,r)}$

We leverage the structure of the matrix of interest T by truncating and decomposing it into a diagonal matrix and k^{th} diagonal and anti-diagonal components.

$$T^{(s,r)} = D + \sum_{k=1}^{s-1} f(k) t^{k[n]} + \sum_{k=1}^{r-1} \left(g(k) a^{k[n]} + g(2^n - k) a^{(2^n - k)[n]} \right), \quad (\text{S29})$$

where

$$D_{ij} = \delta_{ij} \left(d(i) - g(2i) - \sum_{k=1}^{s-1} f(k) q^{k[n]}(i) \right) \quad (\text{S30})$$

$$t_{ij}^{k[n]} = \delta_{|i-j|,k} + \delta_{ij} q^{k[n]}(i), \quad (\text{S31})$$

$$a_{ij}^{k[n]} = \delta_{i+j,k} \quad (\text{S32})$$

and $q^{k[n]}(i)$ are easy to compute classically. Our strategy is to measure the expectation values of each of the $\{D, t^{k[n]}, a^{k[n]}\}$ separately using the induction over n and add them together with the corresponding weights.

C. Measuring D

The expectation values of diagonal matrices with classically easy to compute matrix elements can be measured in one step. Indeed, just measure $|\psi\rangle$ in Z basis and weight the outcomes, i.e. pick $\{V_i\} = \{\mathbb{1}\}$ and $w_{1i} = D_{ii}$.

D. Measuring $t^{k[n]}$ and computing $q^{k[n]}(i)$

We construct $t^{k[n]}$ inductively. The construction is inspired by [2, 3]. The basis of construction is measuring $t^{k[l]}$, where l is the smallest number of qubits that allow for the k -th diagonal

$$l \equiv \lceil \log_2(k+1) \rceil. \quad (\text{S33})$$

Consider a matrix element above the main diagonal with coordinates $(j_1 \dots j_l, p_1 \dots p_l)$. Define l -qubit “+” states

$$|+\rangle_{j_1 \dots j_l, p_1 \dots p_l} = \frac{|j_1 \dots j_l\rangle + |p_1 \dots p_l\rangle}{\sqrt{2}}, \quad \exists i : j_i \neq p_i, \quad (\text{S34})$$

that can be obtained from Z basis states by the circuits on Fig. 1 right.

The projection $|+\rangle_{j_1 \dots j_l, p_1 \dots p_l} \langle +|_{j_1 \dots j_l, p_1 \dots p_l}$ has exactly 1 non-zero matrix element above the main diagonal with coordinates $(j_1 \dots j_l, p_1 \dots p_l)$, one below, and two on the main diagonal of magnitude $1/2$. The binary representation of the row and column positions of these off-diagonal elements differ by at most l bits. Thus, to get the expectation value of $t^{k[l]}$ we need to measure in at most[4] k l -qubit bases containing “+” states.

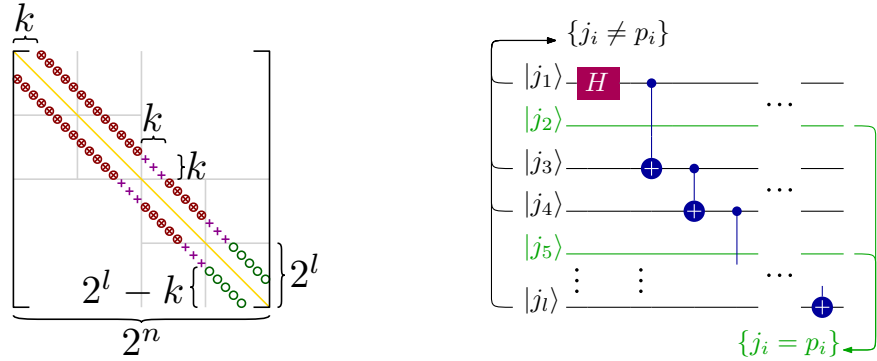


Fig. 1. Left: Measuring $t^{k[n]}$ that includes k^{th} diagonals. Dark green matrix elements denoted by circles \circ are obtained during the basis step, dark red \otimes -denoted elements—via the tensor product and the magenta $+$ —by performing extra measurements in a Bell basis. The measured operator might have some non-zero elements on the diagonal that are easy to compute, denoted by the golden line.

Right: Circuit that prepares $|+\rangle_{j_1 \dots j_l, p_1 \dots p_l} = \frac{|j_1 \dots j_l\rangle + |p_1 \dots p_l\rangle}{\sqrt{2}}$, $\exists i : j_i \neq p_i$ states from the computational basis. The identity circuit acts on the subset of qubits for which $\{j_i = p_i\}$ (green); a version of the GHZ circuit acts on the rest of the qubits.

The step is adding a new qubit. Observe that $\mathbb{1} \otimes t^{k[m]}$ looks almost like $t^{k[m+1]}$. The only missing elements are at the middle of the tensor product matrix, and there are k pairs of them (see magenta $+$ on the Fig. 1 left). How do we get those extra k pairs? Via employing extra measurements in the basis containing “+” states, just like for the basis of the construction.

The complexity of this algorithm to measure the expectation value of $t^{k[n]}$ consists of: [5]

- At most $2^l - k \leq k$ expectation value measurements of projection on “+” states via circuits of depth at most $l + 1$ to obtain $t^{k[l]}$ (see dark green \circ on the Fig. 1).
- Measuring complexity of $\mathbb{1} \otimes t^{k[m]}$ is the same as the measuring complexity of $t^{k[m]}$ (see dark red \otimes on the Fig. 1 left).
- Thus, when adding a new qubit we need to include measurements of at most k projections on “+” states via circuits of depth at most $\lceil \log_2 2k \rceil$. Starting with l qubits, we add $n - l$ qubits (see magenta $+$ on Fig. 1 left).

All together, the number of measurement bases is

$$\text{Comp} \left(t^{k[n]} \right) \leq 2^l - k + (n - l)k \quad (\text{S35})$$

$$< (n + 1 - \log_2 k) k. \quad (\text{S36})$$

In addition to k^{th} diagonals, $t^{k[n]}$ contains extra contributions to matrix elements on the main diagonal $q^{k[n]}(i)$ that have to be accounted for. Fortunately, it is easy to deduce how to compute these contributions from the measurement protocol for $t^{k[n]}$, see Algorithm 1.

Algorithm 1 Computing $q^{k[n]}(i)$ from binary representation of i

```

define  $l \leftarrow \lceil \log_2 (k + 1) \rceil$ ,
last_l_bits  $\leftarrow i \bmod 2^l$ ,
anti_last_l_bits  $\leftarrow 2^l - last\_l\_bits$ ;
initialize output  $\leftarrow 1$ ,
 $j \leftarrow l + 1$ ;
while  $j \leq n$  do
  if  $j^{\text{th}}$  bit of  $i$  is 1 then
    if  $last\_l\_bits < k$  or  $anti\_last\_l\_bits < l$  then
      output  $\rightarrow$  out + 1;
   $j \rightarrow j + 1$ ;
return output.

```

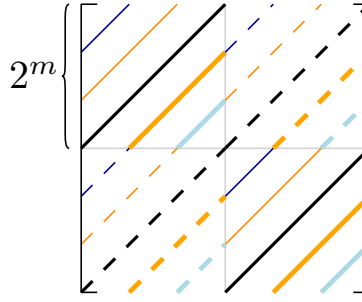


Fig. 2. Measuring the set of anti-diagonals $\{a^{k[m+1]}\}_k$ given a protocol for each of $\{a^{j[m]}\}_j$. Larger k^{th} anti-diagonals can be obtained by taking a tensor product of either $\begin{bmatrix} 1 & 0 \\ 0 & 0 \end{bmatrix}$ or $\begin{bmatrix} 0 & 0 \\ 0 & 1 \end{bmatrix}$ with the k^{th} smaller ones, and for $k \geq 2^m$ additionally combining them with the tensor product of $\begin{bmatrix} 0 & 1 \\ 1 & 0 \end{bmatrix}$ with the $2^m - k^{\text{th}}$ smaller anti-diagonal (dashed lines).

E. Measuring $a^{k[n]}$

We also use inductive construction for the anti-diagonals $a^{k[n]}$. For the basis we need to obtain expectation values of $a^{1[1]} = \begin{bmatrix} 1 & 0 \\ 0 & 0 \end{bmatrix}$, $a^{2[1]} = \begin{bmatrix} 0 & 1 \\ 1 & 0 \end{bmatrix}$ and $a^{3[1]} = \begin{bmatrix} 0 & 0 \\ 0 & 1 \end{bmatrix}$. This can be achieved by sampling one-qubit measurements of ψ in Z to get $\langle a^{1[1]} \rangle_\psi$ and $\langle a^{3[1]} \rangle_\psi$ and in X to get $\langle a^{2[1]} \rangle_\psi$. When measuring in Z , the probability of obtaining \uparrow yields $\langle a^{1[1]} \rangle_\psi$, while the probability of obtaining \downarrow yields $\langle a^{3[1]} \rangle_\psi$.

For the step of the construction (see Fig. 2), observe that

$$a^{k[m+1]} = \begin{cases} a^{1[1]} \otimes a^{k[m]} & \text{for } k \leq 2^m, \\ a^{1[1]} \otimes a^{k[m]} + a^{2[1]} \otimes a^{(-k \bmod 2^m)[m]} & \text{for } 2^m < k < 2 \cdot 2^m, \\ a^{2[1]} \otimes a^{(2^m)[m]} & \text{for } k = 2 \cdot 2^m, \\ a^{3[1]} \otimes a^{(k \bmod 2^m)[m]} + a^{2[1]} \otimes a^{(-k \bmod 2^m)[m]} & \text{for } 2 \cdot 2^m < k \leq 3 \cdot 2^m \\ a^{3[1]} \otimes a^{(k \bmod 2^m)[m]} & \text{for } k < 4 \cdot 2^m. \end{cases} \quad (\text{S37})$$

As such, every time we add a qubit, we (at most) double the number of measurements. Indeed, for $m+1$ qubits we measure the first qubit in Z or X basis, just like for the basis of the construction, and perform the protocol for m qubits on the rest. We would like to get the expectation values that are ϵ -close to the target, so we perform $p-1$ steps for

$$p = \lceil \log_2 r \rceil \sim - \left\lceil \frac{\log_2 \epsilon}{\beta} \right\rceil. \quad (\text{S38})$$

For the conclusion of the construction, we use the rapid decline of the anti-diagonal matrix elements to construct large matrices with only first and last 2^p anti-diagonals being non-zero

$$a^{k[n]} = \begin{cases} \bigotimes_1^{n-p} a^{1[1]} \otimes a^{k[p]} & \text{for } k \leq 2^p, \\ \text{can be neglected} & \text{for } 2^p < k < 2^n - 2^p, \\ \bigotimes_1^{n-p} a^{3[1]} \otimes a^{(k \bmod 2^p)[p]} & \text{for } 2^n - 2^p \leq k. \end{cases} \quad (\text{S39})$$

Thus, we can measure $n-p$ qubits in computational basis and use the step-wise protocol for the rest. We need to take into account only the all- \uparrow and all- \downarrow outputs for the first $n-p$ qubits, yielding upmost and downmost 2^p anti-diagonals. The total number of bases for this protocol is bounded by

$$2^p < 2^{1 - \frac{\log_2 \epsilon}{\beta}} \sim 2\epsilon^{-\frac{1}{\beta}}. \quad (\text{S40})$$

1. Streamlined construction if only upper anti-diagonals are needed

As discussed above, some lower anti-diagonals can be neglected. In this case we can compute all anti-diagonals for $p - 2$ steps and proceed with

$$a^{k[p]} = \begin{cases} a^{1[1]} \otimes a^{k[p-1]} & \text{for } k \leq 2^{p-1}, \\ a^{1[1]} \otimes a^{k[p-1]} + a^{2[1]} \otimes a^{(-k \bmod 2^{p-1})[p]} & \text{for } 2^{p-1} < k < 2^p, \\ a^{2[1]} \otimes a^{(2^{p-1})[p-1]} & \text{for } k = 2^p, \\ \text{can be neglected} & \text{for } 2^p < k; \end{cases} \quad (\text{S41})$$

note that measuring the relevant part of $\{a^{k[p]}\}_{k \leq 2^p}$ requires as many bases as measuring all of $\{a^{k[p-1]}\}_{k=1}^{2^{p-1}}$. Indeed, we supplement the measurement of first 2^{p-1} anti-diagonals by the measurement of an additional qubit in Z basis, and for the other anti-diagonals—in X basis. Finally,

$$a^{k[n]} = \begin{cases} \bigotimes_1^{n-p} a^{1[1]} \otimes a^{k[p]} & \text{for } k \leq 2^p, \\ \text{can be neglected} & \text{for } 2^p < k. \end{cases} \quad (\text{S42})$$

After measuring $n - p$ qubits in computational basis and using the $a^{k[p]}$ protocol for the rest, we need to take into account only the all- \uparrow outputs for the first $n - p$ qubits. This yields upmost 2^p anti-diagonals with the total number of bases for the protocol bounded by

$$2^{p-1} < 2^{-\frac{\log_2 \epsilon}{\beta}} = \epsilon^{-\frac{1}{\beta}}. \quad (\text{S43})$$

F. Complexity of measuring τ

For the quantity of interest

$$\tau = \langle D \rangle + \sum_{k=1}^s f(k) \langle t^{k[n]} \rangle + \sum_{k=1}^r \left[g(k) \langle a^{k[n]} \rangle + g(2^n - k) \langle a^{(2^n - k)[n]} \rangle \right], \quad (\text{S44})$$

$$\text{where } s \sim \epsilon^{-\frac{1}{\alpha}} \text{ and } r \sim \epsilon^{-\frac{1}{\beta}}, \quad (\text{S45})$$

we the we need to measure in at most

$$\text{Comp}(\tau) \leq 1 + \sum_{k=1}^{\sim \epsilon^{-\frac{1}{\alpha}}} (2^l - k + (n - l)k) + 2\epsilon^{-\frac{1}{\beta}} = O \left[\frac{\epsilon^{-\frac{2}{\alpha}} n}{2} + 2\epsilon^{-\frac{1}{\beta}} \right] \quad (\text{S46})$$

number of bases. We need circuits depicted on Fig. 1 of depth at most $\lceil \log_2(2s) \rceil \sim 1 - \frac{\log_2(\epsilon)}{\alpha}$ and to sample at most $O\left(\frac{1}{\sqrt{\epsilon}}\right)$ times per circuit.

3. ADDITIONAL DETAILS OF NUMERICAL VQE RESULTS

A. Vibrational energy levels of Cr_2

The following table is an extended version of table I in main text, including results for a wider range of molecular states.

Electronic state	v	BM	E_v^{VQE}		
			\mathcal{C}_1	$\mathcal{C}_{0.01}$	Linear
${}^1\Sigma_g^+$	0	-15358.94	-15358.87	-15358.99	-15358.99
	1	-14846.67	-14838.70	-14846.75	-14846.96
	2	-14333.21	-14310.29	-14332.80	-14332.82
	3	-13826.93	-13797.65	-13826.87	-13827.29
	4	-13334.02	-13275.12	-13318.77	-13335.45
	5	-12861.37	-12897.70	-12871.32	-12868.75
${}^3\Sigma_u^+$	0	-9862.07	-9861.37	-9862.14	-9862.14
	1	-9559.46	-9538.97	-9556.67	-9559.41
	2	-9300.92	-9240.74	-9266.82	-9300.88
	3	-9080.60	9068.09	-9079.26	-9085.40
	4	-8897.58	-8866.09	-8870.57	-8896.82
	5	-8747.53	-8729.41	-8750.18	...
${}^5\Sigma_g^+$	0	-7566.53	-7565.88	-7566.50	-7566.50
	1	-7416.28	-7397.28	-7416.28	-7416.29
	2	-7264.92	-7181.98	-7264.60	-7264.69
	3	-7114.40	-7075.88	-7117.83	-7118.43
	4	-6965.91	-7001.98	-6953.74	-6958.08
	5	-6820.04	-6873.37	-6837.02	-6840.02
${}^7\Sigma_u^+$	0	-6519.01	-6519.04	-6519.04	-6519.04
	1	-6350.36	-6350.11	-6350.11	-6350.11
	2	-6183.38	-6185.17	-6185.17	-6185.17
	3	-6018.09	-6018.12	-6018.28	-6018.28
	4	-5854.50	-5848.69	-5849.10	-5849.10
	5	-5692.63	-5728.00	-5731.33	-5731.33
${}^9\Sigma_g^+$	0	-5348.79	-5348.82	-5348.82	-5348.82
	1	-5175.81	-5175.51	-5175.51	-5175.51
	2	-5005.17	-5008.55	-5008.56	-5008.56
	3	-4836.85	-4829.80	-4829.92	-4829.92
	4	-4670.91	-4683.42	-4683.68	-4683.68
	5	-4507.31	-4526.72	-4612.83	-4612.83
${}^{11}\Sigma_u^+$	0	-3677.68	-3677.00	-3677.68	-3677.68
	1	-3507.89	-3489.51	-3507.82	-3507.82
	2	-3341.77	-3253.24	-3341.26	-3341.40
	3	-3180.16	-3133.59	-3185.51	-3186.93
	4	-3023.07	-3061.61	-3001.04	-3012.82
	5	-2870.22	-2904.46	-2866.05	-2874.54
${}^{13}\Sigma_g^+$	0	-548.68	-548.65	-548.67	-548.68
	1	-497.16	-496.47	-496.84	-497.15
	2	-449.18	-443.48	-448.36	-449.26
	3	-404.71	-382.88	-390.96	-404.67
	4	-363.58	-369.09	-360.62	-362.99
	5	-325.67	-315.46	-310.29	-325.72

TABLE I. Vibrational energy (in cm^{-1}) of Cr_2 ($v = 0 - 5$) in different electronic states. The benchmark (BM) results are obtained with a converged DVR basis. VQE computations use quantum circuits displayed in Fig. 1 of main text.

B. Optimized quantum circuits for diatomic and triatomic VQE calculations

1. \mathcal{C}_1 and $\mathcal{C}_{0.01}$ ansatzes for Cr_2

Figures 3 and 4 display the 4-qubit \mathcal{C}_1 and $\mathcal{C}_{0.01}$ ansatzes for the seven electronic states of Cr_2 . These circuits are ansatzes obtained using the greedy compositional search and correspond to the simplest circuits that can estimate the 16-point DVR energy with less than 1 cm^{-1} and 0.01 cm^{-1} error respectively. As expected, $\mathcal{C}_{0.01}$ are more complex than the \mathcal{C}_1 circuits and include one or more additional entangling gates. It should also be noted that \mathcal{C}_1 and $\mathcal{C}_{0.01}$ are the same circuit in the case of $^7\Sigma$ and $^9\Sigma$ states, meaning that the smallest ansatz found in the compositional search with an error of less than 1 cm^{-1} from the 16-point DVR ground state energy, also has less than 0.01 cm^{-1} error from the same value.

2. Circuit optimization for triatomics

Figure 5 demonstrates how the VQE error in calculating the ground state energy changes throughout the compositional search. As described in the main text, the ansatz compositional search adds entangling gates to an un-entangled ansatz one at a time, minimizing the VQE-calculated ground state energy at each step. Each of the curves $k = 1, 2, 3, 4$ corresponds to the total number of entangling blocks, as in Eq. (3), considered in the compositional search.

The dashed and dotted lines indicate 1 cm^{-1} and 0.01 cm^{-1} error from the 32-point DVR ground state respectively. The optimized circuits \mathcal{C}_1 and $\mathcal{C}_{0.01}$ which correspond to the simplest circuits found below the dashed and dotted lines are indicated with circles and squares respectively.

3. VQE optimization

In this work, we optimized the ansatz parameters in VQE using the bounded limited memory Broyden, Fletcher, Goldfarb, and Shanno method (L-BFGS-B) [6, 7] and Sequential Least SQuares Programming (SLSQP) [8]. Figure 6 shows the expectation value of the Hamiltonian over the output quantum state of the 5-qubit \mathcal{C}_1 and $\mathcal{C}_{0.01}$ ansatzes of ArHCl during the optimization. Both ansatzes are displayed in the right panel of Fig. (4).

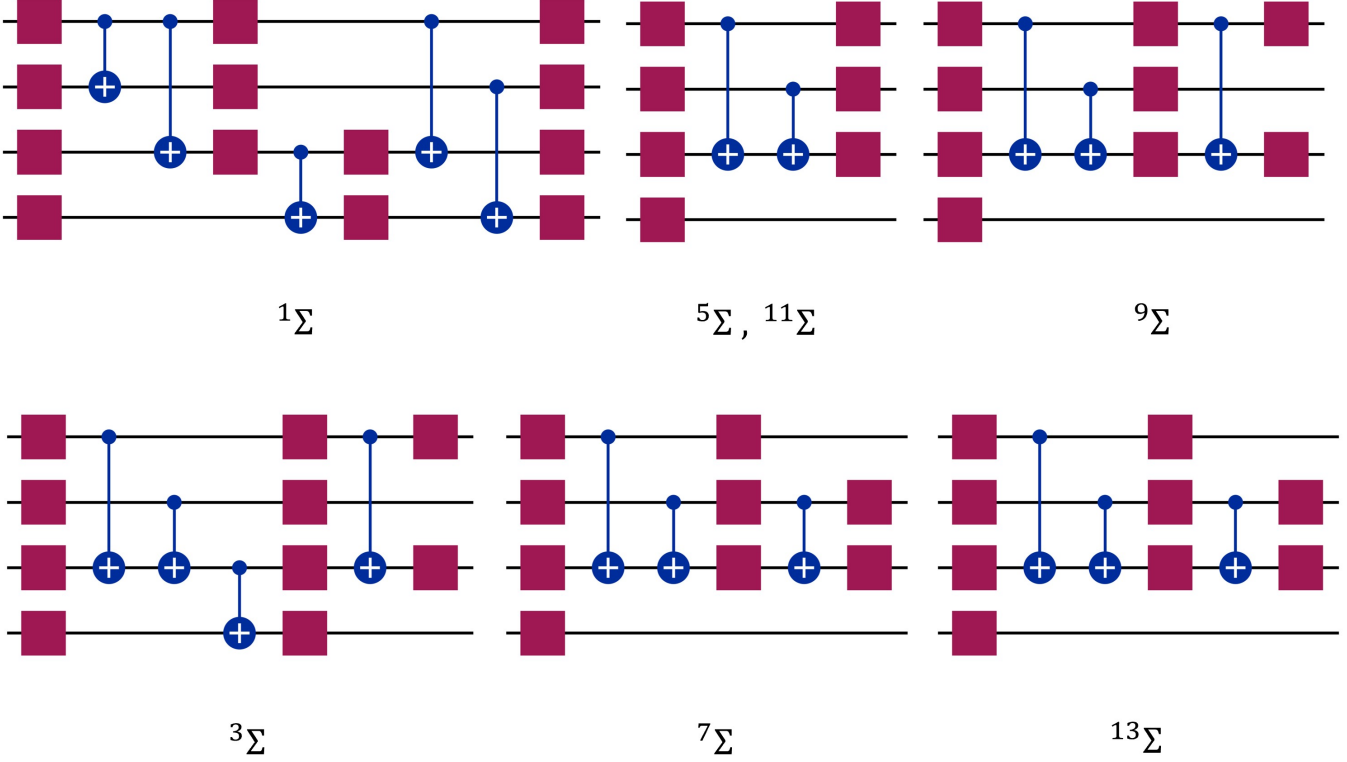


Fig. 3. Quantum circuits for VQE yielding the ground state energy with error $\leq 1 \text{ cm}^{-1}$. The squares represent the R_Y gates and the circles show the entangling CNOT gates.

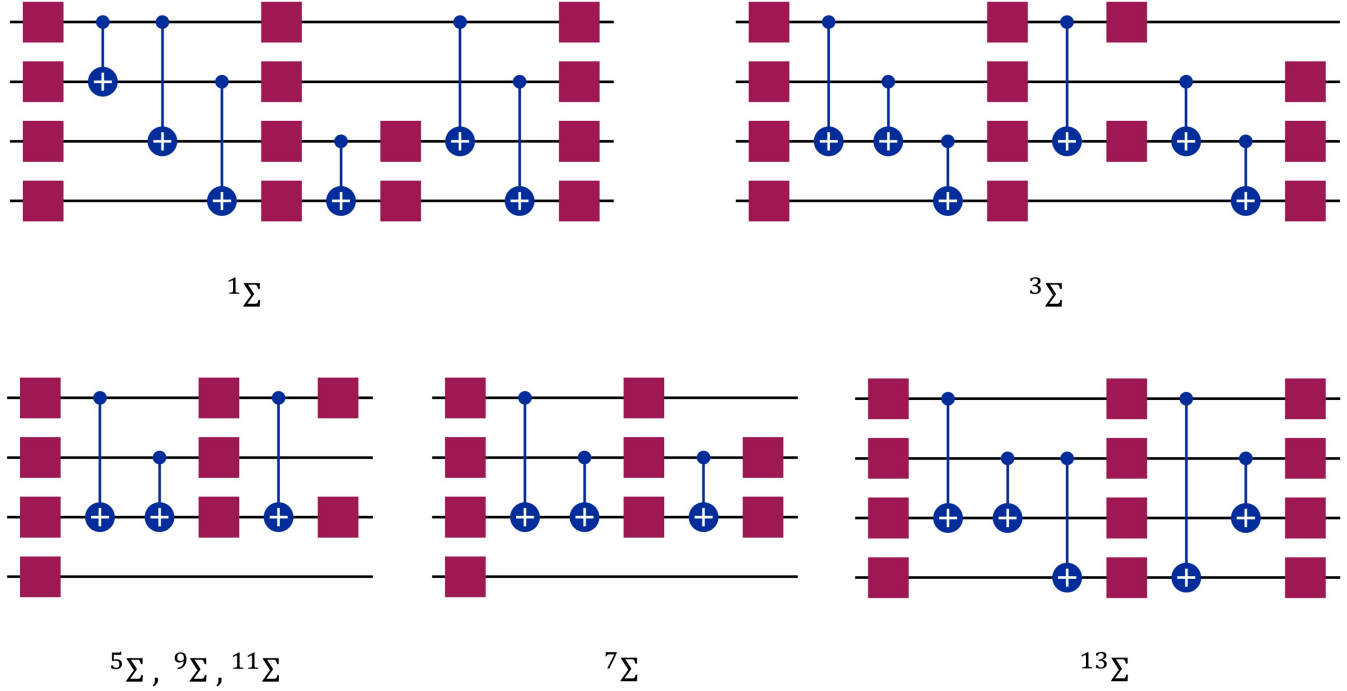


Fig. 4. Quantum circuits for VQE yielding the ground state energy with error $\leq 0.01 \text{ cm}^{-1}$. The squares represent the R_Y gates and the circles show the entangling CNOT gates.

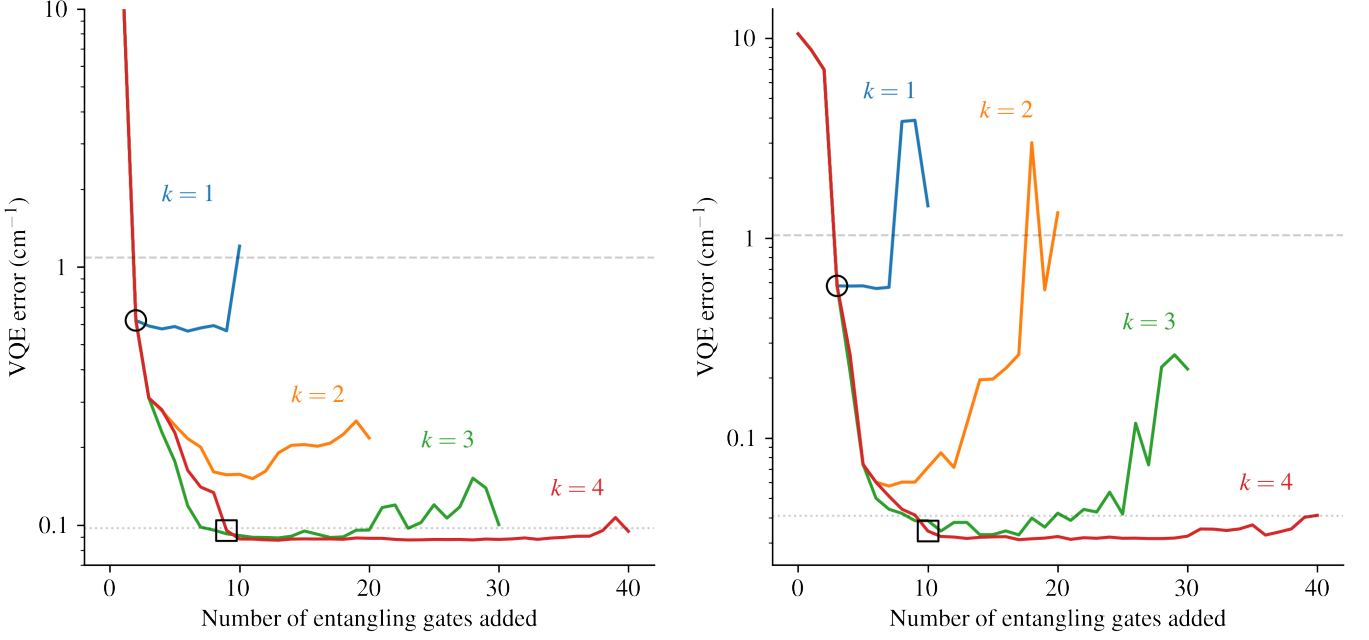


Fig. 5. Error in 5-qubit VQE ground state energy of ArHCl (left) and MgNH (right) in the ansatz composition algorithm with respect to the number of entangling gates added for $k = 1, 2, 3, 4$ ansatz repetitions. Circles indicate \mathcal{C}_1 circuits and squares indicate $\mathcal{C}_{0.01}$ circuits on the optimization graphs.

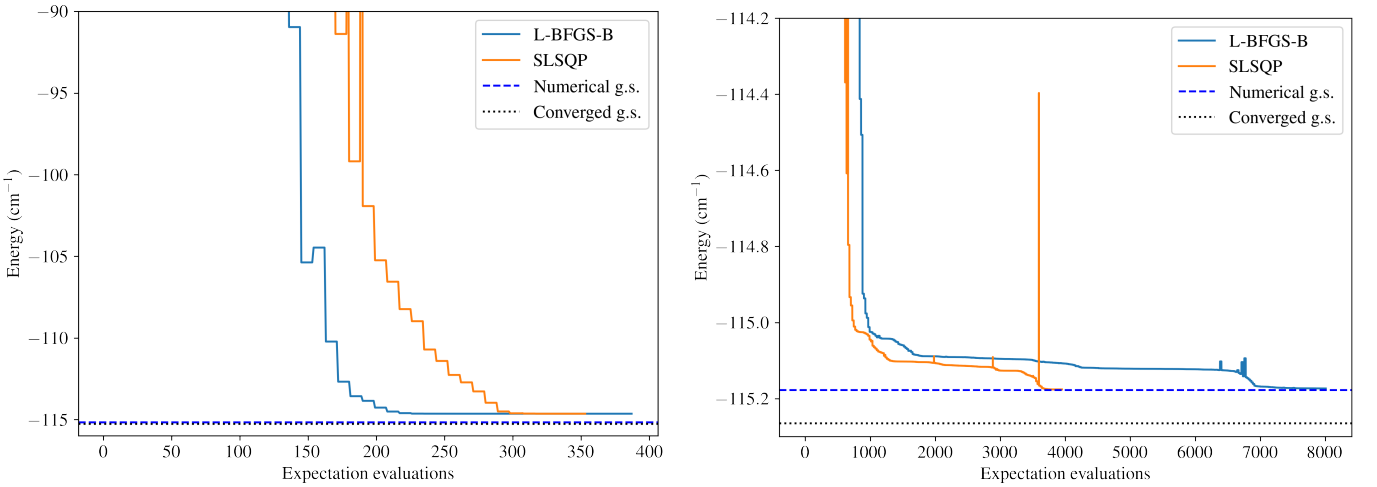


Fig. 6. VQE optimization graphs for 5-qubit \mathcal{C}_1 (left) and $\mathcal{C}_{0.01}$ (right) of ArHCl. The dotted line indicates the converged DVR ground state energy and the dashed line indicates the 32-point DVR ground state energy.

- [1] D. T. Colbert and W. H. Miller, A novel discrete variable representation for quantum mechanical reactive scattering via the S-matrix Kohn method, *J. Chem. Phys.* **96**, 1982 (1992).
- [2] O. Gühne, C.-Y. Lu, W.-B. Gao, and J.-W. Pan, Toolbox for entanglement detection and fidelity estimation, *Phys. Rev. A* **76**, 030305 (2007).
- [3] forkyl40, What is the best way to write a tridiagonal matrix as a linear combination of Pauli matrices?, <https://quantumcomputing.stackexchange.com/questions/23584/what-is-the-best-way-to-write-a-tridiagonal-matrix-as-a-linear-combination-of-pa> (2022), [Online; accessed 20-February-2024].
- [4] The number of need bases might be lower is different pairs of matrix elements can be measured by mapping different computational states to different “+” states with the same circuit.
- [5] This upper bound assumes that we need a separate basis for every pair of off-diagonal elements. The actual complexity may be lower.
- [6] R. H. Byrd, P. Lu, J. Nocedal, and C. Zhu, A limited memory algorithm for bound constrained optimization, *SIAM J. Sci. Comput.* **16**, 1190 (1995).
- [7] C. Zhu, R. H. Byrd, P. Lu, and J. Nocedal, Algorithm 778: L-BFGS-B: Fortran subroutines for large-scale bound-constrained optimization, *ACM Trans. Math. Softw.* **23**, 550–560 (1997).
- [8] D. Kraft, *A Software Package for Sequential Quadratic Programming*, Deutsche Forschungs- und Versuchsanstalt für Luft- und Raumfahrt Köln: Forschungsbericht (Wiss. Berichtswesen d. DFVLR, 1988).